Hadronic medium effects on $Z_{cs}^{-}(3985)$ production in heavy ion collisions

L. M. Abreu* and H. P. L. Vieira†
Instituto de Física, Universidade Federal da Bahia, Campus Universitário de Ondina, 40170-115 Bahia, Brazil

F. S. Navarra‡
Instituto de Física, Universidade de São Paulo, Rua do Matão, 1371, CEP 05508-090 São Paulo, SP, Brazil

(Received 25 August 2022; accepted 16 September 2022; published 3 October 2022)

In this work we study the interactions of the multiquark state $Z_{cs}^{-}(3985)$ with light mesons in a hot hadron gas. Using an effective Lagrangian framework, we estimate the vacuum cross sections as well as the thermal cross sections of the production processes $\bar{D}_s^{(*)}D_s^{(*)} \to Z_{cs}^{-}X(X=\pi,K,\eta)$ and the corresponding inverse reactions. The results indicate that the considered processes have sizeable cross sections. Most importantly, the thermal cross sections for Z_{cs} annihilation are much larger than those for production. This feature might produce relevant effects on some observables, such as the final Z_{cs} multiplicity measured in heavy ion collisions.

DOI: 10.1103/PhysRevD.106.076001

I. INTRODUCTION

Recently, the BES-III Collaboration has observed an excess of events in the K^+ recoil-mass spectrum of the reaction $e^+e^- \to K^+(D_s^{*-}D^0 + D_s^{-}D^{*0})$ for events collected at center-of-mass (CM) energy $\sqrt{s} = 4.681$ GeV, with estimated statistical significance of 5.3σ [1]. By using an amplitude model based on the Breit-Wigner formalism, this peak has been fitted to a resonance with mass and width given by $M = (3982.5^{+1.8}_{-2.6} \pm 2.1)$ MeV, $\Gamma = (12.8^{+5.3}_{-4.4} \pm 3.0)$ MeV, respectively, and has been denoted as $Z_{cs}^{-}(3985)$. Its minimum valence quark content should be most likely $c\bar{c}s\bar{u}$, giving it the status of the first candidate for a charged hidden-charm tetraquark with strangeness.

Since the experimental discovery of the $Z_{cs}^{-}(3985)$ state (or simply Z_{cs}^{-}), the hadron spectroscopy community has been intensely debating its internal structure and the possible mechanisms of its decay and production [2–27]. Because of its proximity to the $D_s^{*-}D^0$ and $D_s^{-}D^{*0}$ thresholds, the hadronic molecular interpretation for the Z_{cs}^{-} seems natural. Along this line, this new state would be the strange partner of the $Z_c(3900)$ [3–9]. Notwithstanding, other possible interpretations have also been proposed, namely, the compact tetraquark configuration resulting from the binding of a diquark and an antidiquark [10,11,13], a virtual pole state [12], a kinematic effect caused by triangle singularities [14,15], a resonance [16], and so on. More experimental and theoretical studies are clearly needed.

A new and promising scenario to investigate the properties of exotic states are heavy ion collisions (HICs). They are characterized by the formation of a locally thermalized state of deconfined quarks and gluons (the quark-gluon plasma or QGP). At the end of the QGP phase, quarks coalesce to form conventional bound states and also exotic states. The latter will exist in a hadron gas and interact with other light hadrons. As pointed out in previous studies, the exotic states can be destroyed in collisions with the comoving light mesons, as well as produced through the inverse processes [28–35]. Their final yields depend on the interaction cross sections, which, in turn, depend on the spatial configuration of the quarks. In the study of the most famous exotic state, the $X(3872)$, it has been shown that the molecular configuration [i.e., the bound state $(D\bar{D}^* + \text{c.c.})$] is larger than a diquark-antidiquark configuration $[(cq)(\bar{c}\,\bar{q})]$ by a factor of about 3–10 [30]. Consequently, meson molecules have larger cross sections and are expected to be more easily produced as well as more easily destroyed than compact tetraquarks in a hadronic medium.

The recent observation of the $X(3872)$ in $Pb-Pb$ collisions at $\sqrt{s_{NN}} = 5.02$ TeV by the CMS Collaboration [36] has opened a new era for the study of exotic states. This observation strengthens our belief that HICs provide

*luciano.abreu@ufba.br
†hildeson.paulo@ufba.br
‡navarra@if.usp.br

a unique and promising experimental environment to study the nature of exotic hadrons.

The present contribution is part of a series of works devoted to the production of exotics states in heavy ion collisions. In the following sections we will analyze the interactions of the Z_{cs}^- state with light mesons. In Sec. II we present our effective Lagrangian formalism. In Sec. III we use it to calculate the Z_{cs}^- production and absorption cross sections and in Sec. IV we compute the corresponding thermal averages. Finally, Sec. V is dedicated to the summary and to the concluding remarks.

II. THE FORMALISM

To understand how the Z_{cs}^- behaves in a surrounding hadronic medium, we will study its interactions with the lightest pseudoscalar mesons π, K, and η. More precisely, we will focus on the reactions $\bar{D}_s^{(*)}D^{(*)} \to Z_{cs}\pi$, $D^{(*)}\bar{D}^{(*)}$, $\bar{D}_s D_s^{(*)} \to Z_{cs}K$, and $\bar{D}_s^{(*)}D^{(*)} \to Z_{cs}\eta$, as well as the inverse processes. In Fig. 1 we present the lowest-order Born diagrams contributing to these processes, without specifying the charge of the particles.

In the evaluation of the reactions in Fig. 1, we make use of the effective theory approach. Consequently, the couplings involving π, $K^{(*)}$, $D^{(*)}$, and $D_s^{(*)}$ mesons are based on the effective formalism in which the vector mesons are identified as dynamical gauge bosons of the hidden $U(N)_V$ local symmetry, and are properly explained in Refs. [28–32]; they read

$$\begin{aligned}
\mathcal{L}_{\pi DD^*} &= ig_{\pi DD^*}D_\mu^*\vec{\tau}\cdot(\bar{D}\partial^\mu\vec{\pi} - \partial^\mu\bar{D}\,\vec{\pi}) + \text{H.c.},\\
\mathcal{L}_{KD_sD^*} &= ig_{KD_sD^*}D_\mu^{*+}(K\partial^\mu D_s - \partial^\mu K D_s) + \text{H.c.},\\
\mathcal{L}_{KDD_s^*} &= ig_{KDD_s^*}D_s^{*\mu}(\partial_\mu D^+ K - D^+\partial_\mu K) + \text{H.c.},\\
\mathcal{L}_{\eta DD^*} &= ig_{\eta DD^*}D_\mu^*(D^+\partial^\mu\eta - \partial^\mu D^+) + \text{H.c.}\\
\mathcal{L}_{\eta D_sD_s^*} &= ig_{\eta D_sD_s^*}D_{s\mu}^*(\partial^\mu D_s^+\eta - \partial_\eta^\mu D_s^+) + \text{H.c.},\\
\mathcal{L}_{\pi D^*D^*} &= -g_{\pi D^*D^*}\epsilon^{\mu\gamma\alpha\beta}\partial_\mu D_\nu^*\vec{\pi}\partial_\alpha D_\beta^{*+},\\
\mathcal{L}_{\eta D^*D^*} &= -g_{\eta D^*D^*}\epsilon^{\mu\nu\alpha\beta}\partial_\mu D_\nu^*\eta\partial_\alpha D_\beta^{*+},\\
\mathcal{L}_{\eta D_s^*D_s^*} &= -g_{\eta D_s^*D_s^*}\epsilon^{\mu\nu\alpha\beta}\partial_\mu D_{s\nu}^*\eta\partial_\alpha D_{s\beta}^*,\\
\mathcal{L}_{KD_s^*D^*} &= g_{KD_s^*D^*}\epsilon^{\mu\nu\alpha\beta}\partial_\mu D_\nu^{*+}K\partial_\alpha D_{s\beta}^* + \text{H.c.},
\end{aligned} \tag{1}$$

where $\vec{\tau}$ are the Pauli matrices in the isospin space; $\vec{\pi}$ denotes the pion isospin triplet; and $D^{(*)} = (D^{(*)0}, D^{(*)+})$ and $K = (K^+, K^0)^T$ represent the isospin doublets for the pseudoscalar (vector) $D^{(*)}$ and K mesons, respectively.

The coupling constants in Eq. (1) describe pseudoscalar-pseudoscalar-vector and vector-vector-pseudoscalar vertices and are given by [29–32]

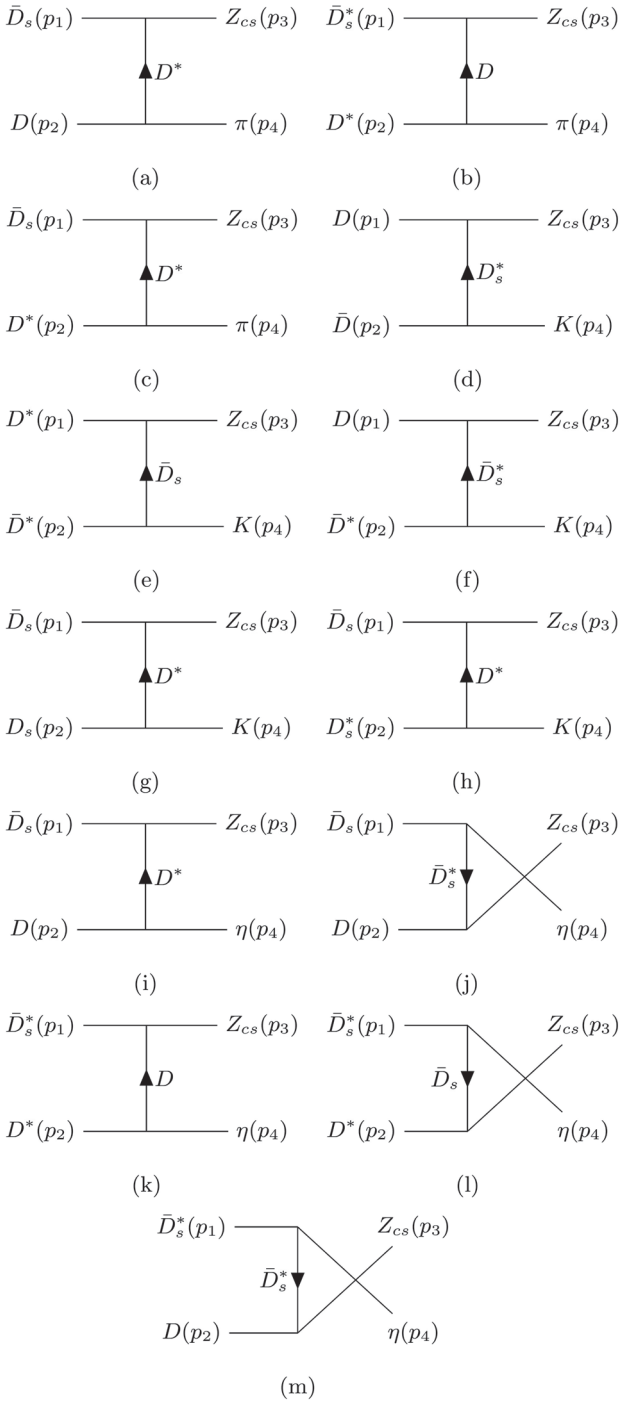

FIG. 1. Diagrams contributing to the following process (without specification of the charges of the particles): $\bar{D}_s^{(*)}D^{(*)} \to Z_{cs}\pi$ [(a)–(c)], $D^{(*)}\bar{D}^{(*)}, \bar{D}_s D_s^{(*)} \to Z_{cs}K$ [(d)–(h)] and $\bar{D}_s^{(*)}D^{(*)} \to Z_{cs}\eta$ [(i)–(m)].

$$\begin{aligned}
g_{\pi DD^*} &= g_{KD_sD^*} = g_{KDD_s^*}\\
&= \sqrt{6}g_{\eta DD^*} = \sqrt{3}g_{\eta D_sD_s^*} \equiv g_{PPV};\\
\sqrt{2}g_{\pi D^*D^*} &= 2\sqrt{3}g_{\eta D^*D^*} = \sqrt{3}g_{\eta D_s^*D_s^*}\\
&= \sqrt{2}g_{KD_s^*D^*} \equiv g_{VVP},
\end{aligned} \tag{2}$$

where

$$g_{PPV} = \frac{m_V}{2f_\pi}\frac{m_{D^*}}{m_{K^*}},$$
$$g_{VVP} = \frac{3m_V^2}{16\pi^2 f_\pi^3}, \tag{3}$$

with m_V being the mass of the vector meson; we take it as the mass of the ρ meson and f_π is the pion decay constant. As pointed in Ref. [29], the factor m_{D^*}/m_{K^*} in the coupling g_{PPV} is introduced in order to reproduce the experimental decay width found for the process $D^* \to D\pi$, and comes from heavy-quark symmetry considerations.

The couplings involving the Z_{cs}^{-} are introduced assuming that it is an S-wave bound state engendered by the superposition of $D_s^{*-}D^0$ and $D_s^{-}D^{*0}$ configurations with quantum numbers $I(J^P) = \frac{1}{2}(1^+)$. As a consequence, the effective Lagrangian describing the interaction between the Z_{cs}^{-} and the $D_s^{*-}D^0$ and $D_s^{-}D^{*0}$ pairs is given by [22]

$$\mathcal{L}_{Z_{cs}} = \frac{g_{Z_{cs}}}{\sqrt{2}} Z_{cs}^{\dagger\mu}(\bar{D}_{s\mu}^{*} D + \bar{D}_s D_\mu^{*}), \tag{4}$$

where Z_{cs} denotes the field associated to Z_{cs}^{-} state; this notation will be used henceforth. Also, the $\bar{D}_{s\mu}^{*}D$ and $\bar{D}_s D_\mu^{*}$ mean the $D_s^{*-}D^0$ and $D_s^{-}D^{*0}$ components, respectively. The effective coupling constant $g_{Z_{cs}}$ is considered to be $g_{Z_{cs}} = 6.0$–6.7 in order to describe the Z_{cs} width, as discussed in Ref. [22].

Based on the effective Lagrangians introduced above, the amplitudes of the processes shown in Fig. 1 can then be calculated. They are given by

$$\begin{aligned}
\mathcal{M}_{\bar{D}_s D\to Z_{cs}\pi} &\equiv \mathcal{M}^{(a)},\\
\mathcal{M}_{\bar{D}_s^{*} D^{*}\to Z_{cs}\pi} &\equiv \mathcal{M}^{(b)},\\
\mathcal{M}_{\bar{D}_s D^{*}\to Z_{cs}\pi} &\equiv \mathcal{M}^{(c)},\\
\mathcal{M}_{D\bar{D}\to Z_{cs}K} &\equiv \mathcal{M}^{(d)},\\
\mathcal{M}_{D^{*}\bar{D}^{*}\to Z_{cs}K} &\equiv \mathcal{M}^{(e)},\\
\mathcal{M}_{D\bar{D}^{*}\to Z_{cs}K} &\equiv \mathcal{M}^{(f)},\\
\mathcal{M}_{\bar{D}_s D_s\to Z_{cs}K} &\equiv \mathcal{M}^{(g)},\\
\mathcal{M}_{\bar{D}_s D_s^{*}\to Z_{cs}K} &\equiv \mathcal{M}^{(h)},\\
\mathcal{M}_{\bar{D}_s D\to Z_{cs}\eta} &\equiv \mathcal{M}^{(i)} + \mathcal{M}^{(j)},\\
\mathcal{M}_{\bar{D}_s^{*} D^{*}\to Z_{cs}\eta} &\equiv \mathcal{M}^{(k)} + \mathcal{M}^{(l)},\\
\mathcal{M}_{\bar{D}_s^{*} D\to Z_{cs}\eta} &\equiv \mathcal{M}^{(m)},
\end{aligned} \tag{5}$$

where the explicit expressions are

$$\begin{aligned}
\mathcal{M}^{(a)} &= \frac{1}{\sqrt{2}}\tau_I g_{Z_{cs}} g_{\pi DD^{*}}(p_2+p_4)^{\mu}\varepsilon_3^{\nu}\frac{1}{t-m_{D^{*}}^2}\\
&\quad\times\left[-g_{\mu\nu}+\frac{(p_1-p_3)_\mu(p_1-p_3)_\nu}{m_{D^{*}}^2}\right],\\
\mathcal{M}^{(b)} &= -\frac{1}{\sqrt{2}}\tau_I g_{Z_{cs}} g_{\pi DD^{*}}\varepsilon_2^{\mu}(2p_4-p_2)_\mu\varepsilon_1^{\nu}\varepsilon_{3\nu}^{*}\frac{1}{t-m_D^2},\\
\mathcal{M}^{(c)} &= \frac{1}{\sqrt{2}}\tau_I g_{Z_{cs}} g_{\pi D^{*}D^{*}}\epsilon^{\mu\nu\alpha\beta}p_{2\mu}p_{4\alpha}\varepsilon_{2\nu}\varepsilon_{3\beta}^{*}\frac{1}{t-m_{D^{*}}^2},\\
\mathcal{M}^{(d)} &= \frac{1}{\sqrt{2}}\tau_{ij} g_{Z_{cs}} g_{KDD_s^{*}}(p_2+p_4)^{\mu}\varepsilon_3^{*\nu}\frac{1}{t-m_{D_s^{*}}^2}\\
&\quad\times\left[-g_{\mu\nu}+\frac{(p_1-p_3)_\mu(p_1-p_3)_\nu}{m_{D_s^{*}}^2}\right],\\
\mathcal{M}^{(e)} &= \frac{1}{\sqrt{2}}\tau_I g_{Z_{cs}} g_{KD_sD^{*}}\varepsilon_2^{\mu}(2p_4-p_2)_\mu\varepsilon_1^{\nu}\varepsilon_{3\nu}^{*}\frac{1}{t-m_{D_s}^2},\\
\mathcal{M}^{(f)} &= \frac{1}{\sqrt{2}}\tau_I g_{Z_{cs}} g_{KD_s^{*}D^{*}}\epsilon^{\mu\nu\alpha\beta}p_{2\mu}p_{4\alpha}\varepsilon_{2\nu}\varepsilon_{3\beta}^{*}\frac{1}{t-m_{D_s^{*}}^2},\\
\mathcal{M}^{(g)} &= \frac{1}{\sqrt{2}}\tau_I g_{Z_{cs}} g_{kD_sD^{*}}(p_2+p_4)^{\mu}\varepsilon_3^{\nu}\frac{1}{t-m_{D^{*}}^2}\\
&\quad\times\left(-g_{\mu\nu}+\frac{(p_1-p_3)_\mu(p_1-p_3)_\nu}{m_{D^{*}}^2}\right),
\end{aligned} \tag{6}$$

and

$$\begin{aligned}
\mathcal{M}^{(h)} &= \frac{1}{\sqrt{2}}\tau_I g_{Z_{cs}} g_{kD_s^{*}D^{*}}\epsilon^{\mu\nu\alpha\beta}p_{2\mu}p_{4\alpha}\varepsilon_{2\nu}\varepsilon_{3\beta}^{*}\frac{1}{t-m_{D^{*}}^2},\\
\mathcal{M}^{(i)} &= \frac{1}{\sqrt{2}}\tau_I g_{Z_{cs}} g_{\eta D^{*}D^{*}}(p_2+p_4)^{\mu}\varepsilon_3^{\nu}\frac{1}{t-m_{D^{*}}^2}\\
&\quad\times\left[-g_{\mu\nu}+\frac{(p_1-p_3)_\mu(p_1-p_3)_\nu}{m_{D^{*}}^2}\right],\\
\mathcal{M}^{(j)} &= -\frac{1}{\sqrt{2}}\tau_I g_{Z_{cs}} g_{\eta D_sD_s^{*}}\frac{1}{u-m_{D_s^{*}}^2}\varepsilon_3^{*\mu}\\
&\quad\times\left[-g_{\mu\nu}+\frac{(p_1-p_4)_\mu(p_1-p_4)_\nu}{m_{D_s^{*}}^2}\right](p_2+p_3)^{\nu},\\
\mathcal{M}^{(k)} &= \frac{1}{\sqrt{2}}\tau_I g_{Z_{cs}} g_{\eta DD^{*}}\varepsilon_2^{\mu}(2p_2-p_4)_\mu\varepsilon_1^{\nu}\varepsilon_{3\nu}^{*}\frac{1}{t-m_D^2},\\
\mathcal{M}^{(l)} &= \frac{1}{\sqrt{2}}\tau_I g_{Z_{cs}} g_{\eta D_sD_s^{*}}\varepsilon_3^{*\mu}\varepsilon_1^{\nu}\varepsilon_{2\mu}\frac{1}{u-m_{D_s}^2}(2p_4-p_1)_\nu,\\
\mathcal{M}^{(m)} &= \frac{1}{\sqrt{2}}\tau_I g_{Z_{cs}} g_{\eta D_s^{*}D_s^{*}}\epsilon^{\mu\nu\alpha\beta}p_{1\mu}\varepsilon_{1\nu}p_{4\alpha}\varepsilon_{3\beta}^{*}\frac{1}{u-m_{D_s^{*}}^2},
\end{aligned} \tag{7}$$

where τ_I is the isospin factor related to part of the particles in the vertices PPV and VVP; $p_1(p_3)$ and $p_2(p_4)$ are the momenta of initial (final) state particles, and t, u are two of the Mandelstam variables: $s = (p_1+p_2)^2$, $t = (p_1-p_3)^2$, and $u = (p_1-p_4)^2$.

TABLE I. Isospin coefficients τ_I of the processes described in Eq. (5) by considering the charges Q_{1f} and Q_{2f} for each one of the two particles in final state.

Process	Vertices	(Q_{1f}, Q_{2f})	τ_{ij}
(a)	$D^{0,+}D^{*0}\pi^{0,+}$	$(-,0)$	$\frac{1}{\sqrt{2}}$
		$(-,+)$	1
(b)	$D^{*0,+}D^{0}\pi^{0,+}$	$(-,0)$	$-\frac{1}{\sqrt{2}}$
		$(-,+)$	-1
(c)	$D^{*0,+}D^{*0}\pi^{0,+}$	$(-,0)$	$\frac{1}{\sqrt{2}}$
		$(-,+)$	1
(d)	$\bar{D}^{0,-}D_s^{*-}K^{0,+}$	$(-,0)$	-1
		$(-,+)$	-1
(e)	$\bar{D}^{*0,-}D_s^{*-}K^{0,+}$	$(-,0)$	-1
		$(-,+)$	-1
(f)	$\bar{D}^{*0,-}D_s^{*-}K^{0,+}$	$(-,0)$	-1
		$(-,+)$	-1
(g)	$D_s^{+}D^{*0}K^{+}$	$(-,+)$	-1
(h)	$D_s^{*+}D^{*0}K^{+}$	$(-,+)$	-1
(i)	$D^{0}D_s^{*0}\eta^{0}$	$(-,0)$	$-\frac{\sqrt{6}}{3}$
(j)	$D_s^{-}D^{*-}\eta^{0}$		-1
(k)	$D^{*0}D_s^{0}\eta^{0}$	$(-,0)$	$-\frac{\sqrt{6}}{3}$
(l)	$D_s^{*-}D_s^{-}\eta^{0}$		-1
(m)	$D_s^{*-}D_s^{*-}\eta^{0}$	$(-,0)$	1

The isospin coefficients τ_I of the reactions listed in Eq. (5) are determined by considering the charges Q_{1f} and Q_{2f} for each of the two particles in final state, whose combination gives the total charge $Q = Q_{1f} + Q_{2f} = 0, -1$. There are two possible charge configurations (Q_{1f}, Q_{2f}) for each process in Eq. (5). The values of $\tau_I^{(i)}$ for the possible configurations are listed in Table I.

III. CROSS SECTIONS

The isospin-spin-averaged cross section in the CM frame for the processes in Eq. (5) is given by

$$\sigma_{ab\to cd}(s) = \frac{1}{64\pi^2 s}\frac{|\vec{p}_{cd}|}{|\vec{p}_{ab}|}\int d\Omega \overline{\sum_{S,I}}|\mathcal{M}_{ab\to cd}(s,\theta)|^2 F^4, \quad (8)$$

where $\sqrt{s}$ is the CM energy; $|\vec{p}_{ab}|$ and $|\vec{p}_{cd}|$ stand for the three-momenta of initial and final particles in the CM frame, respectively; the symbol $\overline{\sum_{S,I}}$ denotes the sum over the spins and isospins of the particles in the initial and final state, weighted by the isospin and spin degeneracy factors $g_{1i,r} = (2I_{1i,r}+1)(2I_{2i,r}+1)$ and $g_{2i,r} = (2S_{1i,r}+1)(2S_{2i,r}+1)$ of the two particles forming the initial state, namely:

$$\overline{\sum_{S,I}}|\mathcal{M}_{ab\to cd}|^2 \equiv \frac{1}{g_a g_b}\sum_{S,I}|\mathcal{M}_{ab\to cd}|^2 = \frac{1}{g_a g_b}\sum_{(Q_1,Q_2)}\left[\sum_S |\mathcal{M}^{(Q_1,Q_2)}_{ab\to cd}|^2\right]. \quad (9)$$

Finally, as usual, we have introduced the form factor F to account for the composite nature of hadrons and their finite extension observed at increasing momentum transfers. The form factor introduces a suppression of the high momentum region and therefore tames the artificial growth of the cross sections. We make use of a monopolelike expression, defined as [33,34]

$$F(\vec{q}) = \frac{\Lambda^2}{\Lambda^2 + \vec{q}^2}, \quad (10)$$

with $\vec{q}$ being the momentum of the exchanged particle in a t or u channel in the center-of-mass frame, and Λ the cutoff, chosen to be in the range $m_{\rm min} < \Lambda < m_{\rm max}$, taking $m_{\rm min}$ ($m_{\rm max}$) as the mass of the lightest (heaviest) particle entering or exiting the vertices. In the present approach we fix $\Lambda = 2.0$ GeV. For a detailed discussion on the role and choice of the form factor, we refer the reader to Ref. [34].

Using the detailed balance relation, we can also evaluate the cross sections of the inverse processes, which lead to the absorption of the Z_{cs}^- state.

The calculations of the present work are done with the isospin-averaged masses reported in the Particle Data Group [37]. Since we use a range of values for the coupling $g_{Z_{cs}}$ (in order to take into account the uncertainties), the results are shown in terms of bands.

The cross sections for the Z_{cs}^- production as functions of the CM energy $\sqrt{s}$ are plotted in Fig. 2. Excluding the contribution of the channel $D_s^* D^* \to Z_{cs}\pi$, all the cross sections are endothermic, having a substantial increase near the threshold and after that a weak dependence on $\sqrt{s}$. In the region close to the threshold we note that the distinct channels present magnitudes of the order of $\sim 10^{-4} - 10^{-2}$ mb. For the Z_{cs}^- production induced by kaon and η mesons, the channels with final states $D_s\bar{D}_s^*$ and $D_s\bar{D}_s$ have maximal cross sections at smaller CM energies. This pattern remains at moderate CM energies (i.e., 500 MeV above the threshold) for the channels involving the $Z_{cs}K$, η production, whereas those of $Z_{cs}\pi$ have closer magnitudes.

Let us now examine the inverse processes. Their cross sections as functions of the CM energy $\sqrt{s}$ are plotted in Fig. 3. We see that all these absorption cross sections are exothermic, becoming very large near the threshold. The exception is the case of $Z_{cs}\pi \to \bar{D}_s^* D^*$, which has a distinct behavior: it starts small at the threshold but rapidly increases and becomes very large, and after that decreases as in the other cases. From the region close to the threshold

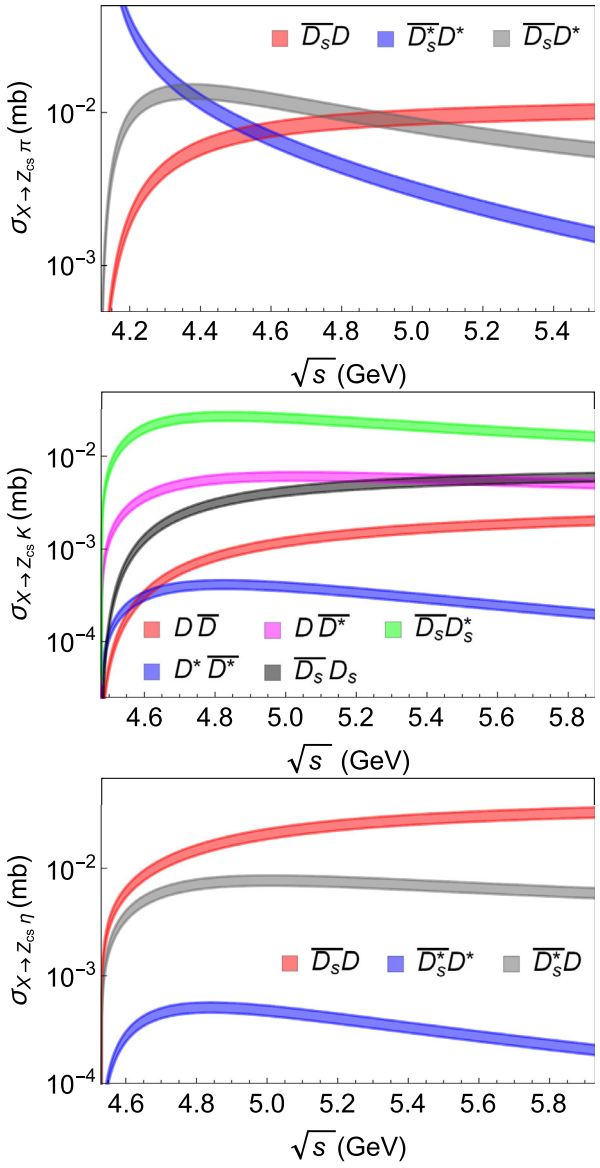

FIG. 2. Cross sections for the production processes $Z_{cs}^-\pi$ (top), Z_{cs}^-K (center), and $Z_{cs}^-\eta$ (bottom), as functions of $\sqrt{s}$.

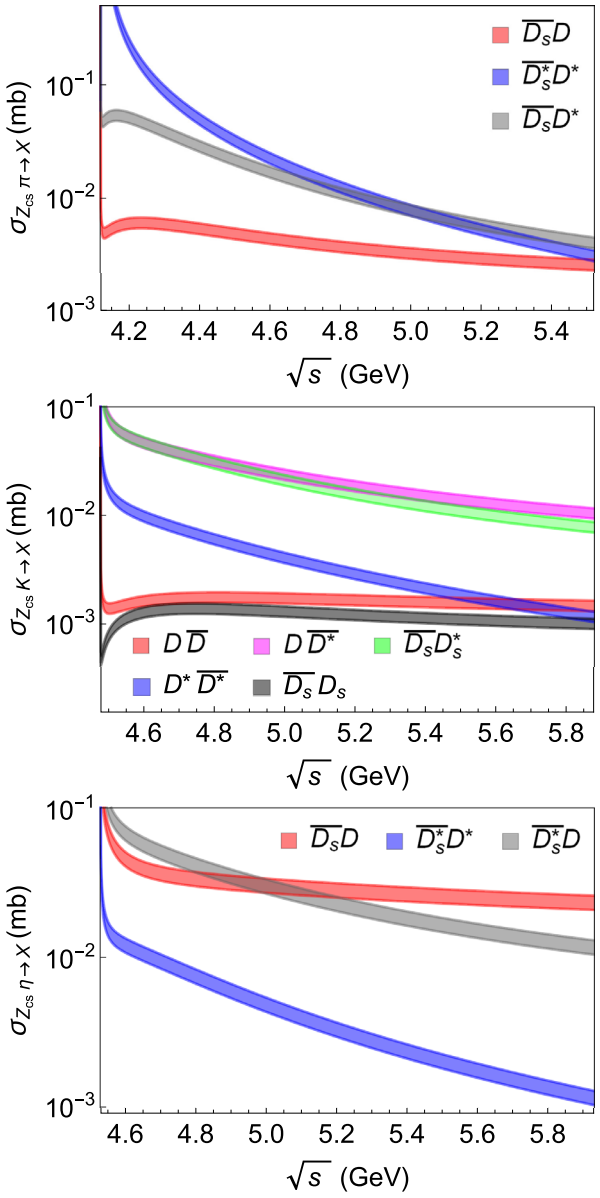

FIG. 3. Cross sections for the absorption processes $Z_{cs}^-\pi$ (top), Z_{cs}^-K (center), and $Z_{cs}^-\eta$ (bottom), as functions of $\sqrt{s}$. The behavior of the reaction $\bar{D}_s^* D^* \to Z_{cs}\pi$ near the threshold is evidenced in the inlay panel at the top.

up to moderate energies, we observe that the cross sections are of the order $\sim 10^{-3} - 10^{-1}$ mb.

The comparison between Z_{cs}^- absorption and production by comoving light mesons can be done more easily when the different contributions are added up. The total cross sections for All $\to Z_{cs}^- X$ and $Z_{cs}^- X \to$ All$(X = \pi, K, \eta)$ as functions of $\sqrt{s} - \sqrt{s_0}$ ($\sqrt{s_0}$ being the mass threshold for each channel) are plotted in Fig. 4. The results suggest that the cross sections $\sigma_{\text{All}\to Z_{cs}^- X}$ have similar magnitude and a weak dependence on $\sqrt{s} - \sqrt{s_0}$. This fact reflects the dynamics as well as the choice of the values of the coupling constants. In the case of absorption processes, this similarity is less pronounced and the dependence with $\sqrt{s} - \sqrt{s_0}$ is stronger.

The most important information contained in Fig. 4 is that, for the energy values which are more relevant to heavy ion collisions ($\sqrt{s} - \sqrt{s_0} < 0.6$ GeV), $\sigma_{Z_{cs}^- X\to \text{All}} > \sigma_{\text{All}\to Z_{cs}^- X}$, i.e., the absorption cross sections are greater than the production ones.

In order to better understand this behavior it is useful to rewrite the ratio of momenta in Eq. (8) in an expanded and more instructive form as

$$\frac{|\vec{p}_{cd}|}{|\vec{p}_{ab}|} = \left(\frac{[s-(m_c+m_d)^2][s-(m_c-m_d)^2]}{[s-(m_a+m_b)^2][s-(m_a-m_b)^2]}\right)^{1/2}. \tag{11}$$

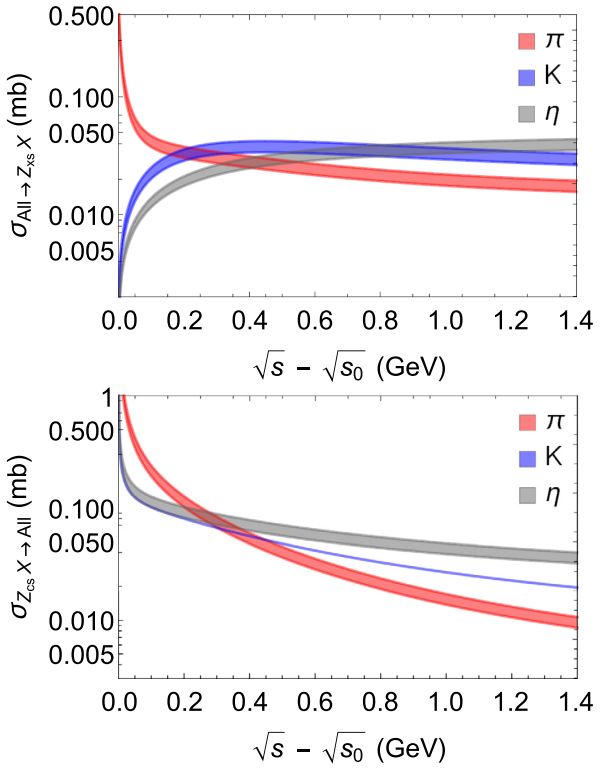

FIG. 4. Sum of all cross sections for $\text{All} \to Z_{cs}^- X$ (top) and $Z_{cs}^- X \to \text{All}$ (bottom), where $X = \pi$, K and η, in function of $\sqrt{s} - \sqrt{s_0}$.

Now let us consider the processes with the largest cross sections: $Z_{cs}\pi \to \bar{D}_s^* D^*$ and the corresponding inverse process $\bar{D}_s^* D^* \to Z_{cs}\pi$. Assuming, just for the sake of the discussion, that $m_\pi = 0$, $m_{\bar{D}_s^*} = m_{D^*} = m$ and $m_{Z_{cs}} = 2m$, and substituting these masses in (11), we find that the ratio is $\sqrt{s/(s-4m^2)}$ for Z_{cs} absorption and it is $\sqrt{(s-4m^2)/s}$ for Z_{cs} production. We see then that the difference of these two processes comes to a large extent from the phase space and can be big.

Apart from the ratio of momenta, differences can also be due to the degeneracy factors. In the absorption process, the initial state is the $Z_{cs} - \pi$ system, for which the isospin (g_I), spin (g_S), and total (g_T^a) degeneracy factors are

$$g_T^a = g_I^Z(=2) \times g_S^Z(=3) \times g_I^\pi(=3) \times g_S^\pi(=1) = 18. \quad (12)$$

For the production process, we have $\bar{D}_s^*$ and D^* in the initial state and the corresponding degeneracy factors are

$$g_T^p = g_I^{D_s^*}(=1) \times g_S^{D_s^*}(=3) \times g_I^{D^*}(=2) \times g_S^{D^*}(=3) = 18. \quad (13)$$

In this example $g_T^a = g_T^p$ and the difference between absorption and production comes solely from the phase space. However, in other process g_T^a and g_T^p can differ by 1 order of magnitude.

IV. THERMAL CROSS SECTIONS

Motivated by the results of the previous section, we turn our attention to the heavy ion collision environment. Keeping in mind that the temperature of the hadronic medium drives the collision energy, it is convenient to evaluate the thermal cross sections, defined as convolutions of the vacuum cross sections with thermal momentum distributions of the colliding particles. This thermal average leads to a strong suppression of the kinematical configurations very close to the thresholds, and therefore threshold effects will not play a relevant role in the presence of a hot hadronic medium.

The cross section averaged over the thermal distribution for a reaction involving an initial two-particle state going into two final particles $ab \to cd$ is given by [28,30–32,38]

$$\begin{aligned}\langle \sigma_{ab\to cd} v_{ab} \rangle &= \frac{\int d^3\mathbf{p}_a d^3\mathbf{p}_b f_a(\mathbf{p}_a) f_b(\mathbf{p}_b) \sigma_{ab\to cd} v_{ab}}{\int d^3\mathbf{p}_a d^3\mathbf{p}_b f_a(\mathbf{p}_a) f_b(\mathbf{p}_b)} \\ &= \frac{1}{4\beta_a^2 K_2(\beta_a)\beta_b^2 K_2(\beta_b)} \\ &\quad \times \int_{z_0}^\infty dz K_1(z) \sigma(s = z^2 T^2) \\ &\quad \times [z^2 - (\beta_a + \beta_b)^2][z^2 - (\beta_a - \beta_b)^2] \quad (14)\end{aligned}$$

where v_{ab} denotes the relative velocity of the two initial interacting particles; the function $f_i(\mathbf{p}_i)$ is the Bose-Einstein distribution; $\beta_i = m_i/T$ (T being the temperature); $z_0 = \max(\beta_a + \beta_b, \beta_c + \beta_d)$, and K_1 and K_2 are the modified Bessel functions of the second kind.

In Figs. 5 and 6 we show the thermal cross sections for Z_{cs} production and absorption plotted as functions of the temperature. The results reveal that, in general, the thermal cross sections for the Z_{cs} absorption do not change much in this range of temperature, staying almost constant. On the other hand, in the case of Z_{cs} production, most of the cross sections grow significantly with the temperature.

These features can be understood from the energy dependence of the cross sections shown in Figs. 2 and 3. As it can be seen, all the cross sections (with one exception) of Z_{cs} production grow with the CM energy and as the temperature increases and the charmed mesons in initial state become more energetic (surpassing the threshold), the thermal production cross sections grow with T.

We emphasize that our most important result is that the thermal cross sections for Z_{cs} absorption are greater than those for production, at least by 1 order of magnitude. For instance, the cross section of $Z_{cs}\pi \to \bar{D}_s^* D^*$ is bigger than that for the corresponding inverse reaction by 1 order of magnitude; in the case of the channel $Z_{cs}K \to D_s\bar{D}_s$ and its inverse, this difference is at least of 2 orders of magnitude, depending on the temperature.

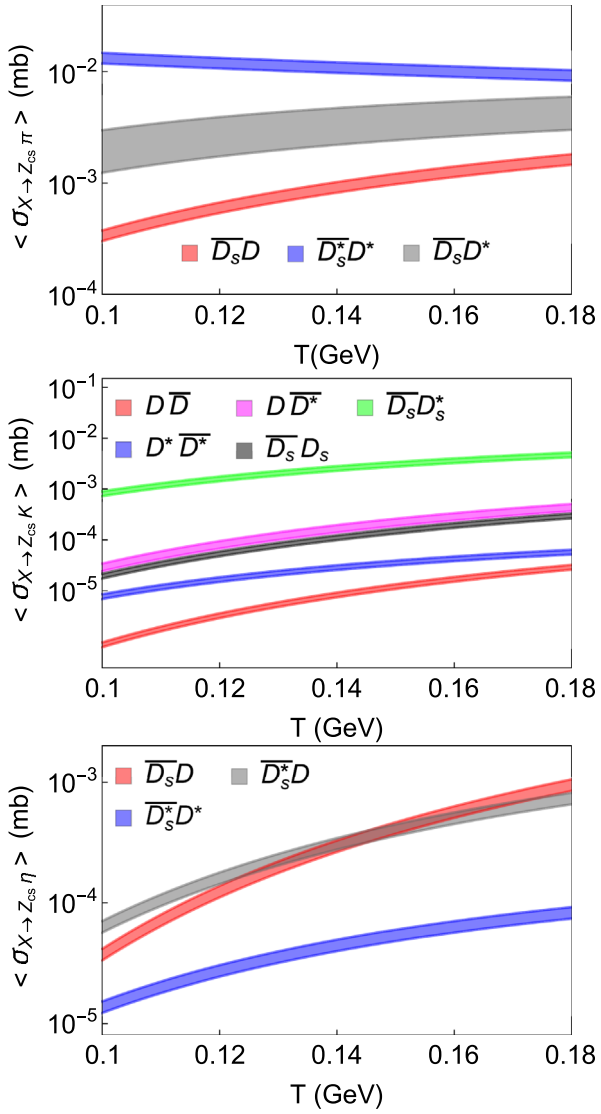

FIG. 5. Thermal cross sections for the production processes $Z_{cs}^{-}\pi$ (top), $Z_{cs}^{-}K$ (center), and $Z_{cs}^{-}\eta$ (bottom), as a function of temperature T.

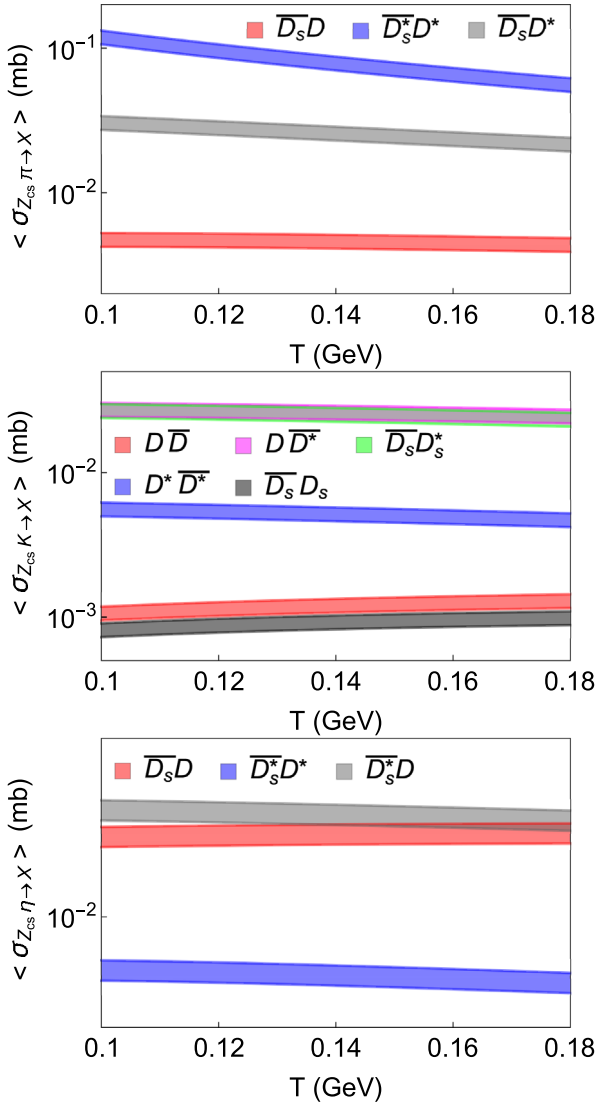

FIG. 6. Thermal cross sections for the absorption processes $Z_{cs}^{-}\pi$ (top), $Z_{cs}^{-}K$ (center), and $Z_{cs}^{-}\eta$ (bottom), as a function of temperature T.

This result might have important implications for the observed final yield of the Z_{cs} state in heavy ion collisions. The Z_{cs} multiplicity at the end of the quark-gluon plasma phase (which may be estimated via the coalescence model) might go through sizeable changes because of the interactions during the hadron gas phase. The different magnitudes of the thermal cross sections for the Z_{cs} annihilation and production by comoving hadrons might lead to a suppression of Z_{cs}.

V. CONCLUDING REMARKS

In this work we have investigated the interactions of the multiquark state Z_{cs} with light mesons in the hadron gas phase. We made use of an effective Lagrangian framework. The vacuum cross sections as well as the thermal cross sections for the $Z_{cs}X-$ absorption and production processes ($X = \pi$, K, η) have been estimated.

Our results have uncertainties coming from the couplings constants and from the form factors (with the corresponding cutoff). Nevertheless, they clearly show that the thermal cross sections for Z_{cs} annihilation are larger than the corresponding ones for production. It would be tempting to conclude that there will be a reduction of the multiplicity of this state due to the absorption by the hadron gas. However, in the rate equation which controls the evolution of the Z_{cs} abundance there are gain and loss terms and they depend on the initial number of $D^{(*)}$'s and $D_s^{(*)}$'s. Since these mesons are much more abundant than the Z_{cs}'s, it is not clear *a priori* what will be the final outcome.

A similar feature was also observed in other multiquark states, such as the T_{cc}^{+}. In this case, it was observed in [35] that the rise or fall of the initial abundance depended on several factors, including the internal structure (compact tetraquark or large meson molecule). This is certainly a very interesting question and work in this direction is already in progress.

ACKNOWLEDGMENTS

The authors would like to thank the Brazilian funding agencies for their financial support: CNPq (LMA: Contracts No. 309950/2020-1 and No. 400546/2016-7), FAPESB (LMA: Contract No. INT0007/2016). We are also grateful to the INCT-FNA.

[1] M. Ablikim *et al.* (BESIII Collaboration), Phys. Rev. Lett. **126**, 102001 (2021).
[2] S. H. Lee, M. Nielsen, and U. Wiedner, J. Korean Phys. Soc. **55**, 424 (2009).
[3] Z. Yang, X. Cao, F. K. Guo, J. Nieves, and M. P. Valderrama, Phys. Rev. D **103**, 074029 (2021).
[4] L. Meng, B. Wang, and S. L. Zhu, Phys. Rev. D **102**, 111502 (2020).
[5] Z. F. Sun and C. W. Xiao, arXiv:2011.09404.
[6] B. Wang, L. Meng, and S. L. Zhu, Phys. Rev. D **103**, L021501 (2021).
[7] Y. J. Xu, Y. L. Liu, C. Y. Cui, and M. Q. Huang, Phys. Rev. D **104**, 094028 (2021).
[8] M. J. Yan, F. Z. Peng, M. Sánchez Sánchez, and M. Pavon Valderrama, Phys. Rev. D **104**, 114025 (2021).
[9] P. G. Ortega, D. R. Entem, and F. Fernandez, Phys. Lett. B **818**, 136382 (2021).
[10] Z. G. Wang, Chin. Phys. C **45**, 073107 (2021).
[11] X. Jin, Y. Wu, X. Liu, Y. Xue, H. Huang, J. Ping, and B. Zhong, Eur. Phys. J. C **81**, 1108 (2021).
[12] P. G. Ortega, D. R. Entem, and F. Fernandez, arXiv:2112.08038.
[13] H. Garcilazo and A. Valcarce, Symmetry **13**, 1171 (2021).
[14] N. Ikeno, R. Molina, and E. Oset, Phys. Lett. B **814**, 136120 (2021).
[15] F. J. Llanes-Estrada and L. M. Abreu, *Proc. Sci.*, EPS-HEP2021 (2022) 278 [arXiv:2110.07438].
[16] M. L. Du, M. Albaladejo, F. K. Guo, and J. Nieves, arXiv:2201.08253.
[17] J. Z. Wang, Q. S. Zhou, X. Liu, and T. Matsuki, Eur. Phys. J. C **81**, 51 (2021).
[18] R. Chen and Q. Huang, Phys. Rev. D **103**, 034008 (2021).
[19] K. Azizi and N. Er, Eur. Phys. J. C **81**, 61 (2021).
[20] J. Y. Süngü, A. Türkan, H. Sundu, and E. V. Veliev, Eur. Phys. J. C **82**, 453 (2022).
[21] M. Z. Liu, J. X. Lu, T. W. Wu, J. J. Xie, and L. S. Geng, arXiv:2011.08720.
[22] Q. Wu and D. Y. Chen, Phys. Rev. D **104**, 074011 (2021).
[23] J. Ferretti and E. Santopinto, Sci. Bull. **67**, 1209 (2022).
[24] N. Ikeno, R. Molina, and E. Oset, Phys. Rev. D **105**, 014012 (2022).
[25] Q. Wu, D. Y. Chen, W. H. Qin, and G. Li, Eur. Phys. J. C **82**, 520 (2022).
[26] H. Chen, Q. Huang, and R. G. Ping, Phys. Rev. D **105**, 036002 (2022).
[27] S. Han and L. Y. Xiao, Phys. Rev. D **105**, 054008 (2022).
[28] S. Cho and S. H. Lee, Phys. Rev. C **88**, 054901 (2013).
[29] A. Martinez Torres, K. P. Khemchandani, F. S. Navarra, M. Nielsen, and L. M. Abreu, Phys. Rev. D **90**, 114023 (2014); A. Martinez Torres, K. P. Khemchandani, F. S. Navarra, M. Nielsen, and L. M. Abreu, Acta Phys. Pol. B Proc. Suppl. **8**, 247 (2015).
[30] L. M. Abreu, K. P. Khemchandani, A. Martinez Torres, F. S. Navarra, and M. Nielsen, Phys. Lett. B **761**, 303 (2016).
[31] L. M. Abreu, K. P. Khemchandani, A. Martínez Torres, F. S. Navarra, and M. Nielsen, Phys. Rev. C **97**, 044902 (2018).
[32] L. M. Abreu, F. S. Navarra, and M. Nielsen, Phys. Rev. C **101**, 014906 (2020).
[33] J. Hong, S. Cho, T. Song, and S. H. Lee, Phys. Rev. C **98**, 014913 (2018).
[34] L. M. Abreu, F. S. Navarra, M. Nielsen, and H. P. L. Vieira, Eur. Phys. J. C **82**, 296 (2022).
[35] L. M. Abreu, F. S. Navarra, and H. P. L. Vieira, Phys. Rev. D **105**, 116029 (2022).
[36] A. M. Sirunyan *et al.* (CMS Collaboration), Phys. Rev. Lett. **128**, 032001 (2022).
[37] P. A. Zyla *et al.* (Particle Data Group), Prog. Theor. Exp. Phys. **2020**, 083C01 (2020).
[38] P. Koch, B. Muller, and J. Rafelski, Phys. Rep. **142**, 167 (1986).